# A post-combustion carbon capture process by amines supported on solid pellets - with estimation of kinetic parameters

Luigi Bisone,[†] Sergio Bittanti,[‡] Silvia Canevese,[*,†] Antonio De Marco,[†] Simone Garatti,[‡] Maurizio Notaro,[†,¶] and Valter Prandoni[†]

*RSE S.p.A. (Ricerca sul Sistema Energetico), 20134, Milan, Italy, Dipartimento di Elettronica, Informazione e Bioingegneria, Politecnico di Milano, Piazza Leonardo da Vinci 32, 20133, Milan, Italy, and "Processes and catalytic materials" Laboratory, RSE S.p.A., 20134, Milan, Italy*

E-mail: canevese@rse-web.it

Phone: +39 02 39925696. Fax: +39 02 39925626

[*]To whom correspondence should be addressed
[†]RSE S.p.A.
[‡]Politecnico di Milano
[¶]RSE Laboratory

# 1 Introduction

Chemical absorption by aqueous alkanolamine solvents[1,2] is a viable near-term technology for post-combustion $CO_2$ capture from power plants flue gases.[3] However, it has a number of drawbacks, such as corrosion,[4,5] foam formation[6] and amine degradation due to oxidation mechanisms.[7] Moreover, it is highly energy intensive, especially in the sorbent regeneration stage: typical energy penalties with monoethanolamine (MEA) or diethanolamine (DEA) processes range from 15 to 37% of the plant net power output.[2,8] Therefore, many research efforts have been devoted to conceive different kinds of technologies.[9,10] Several *solid* sorbents, in particular, with or without amines, have been tested.[11–15] Solid sorbents can achieve both higher gas absorption rate and larger absorption capacity. Moreover, they have both lower heat capacity and lower regeneration temperature and thus allow an energy consumption reduction.

In this work, we focus on an innovative process[16] based on chemical absorption by DEA supported on highly porous solid alumina pellets.[17–19] The proposed absorbent is low cost, has high $CO_2$ selectivity, high absorption capacity and low specific heat,[20] with, of course, good amine stability with respect to oxidative degradation and corrosion.

The configuration of the considered $CO_2$ capture process[21] is based on a fixed-bed absorption/desorption diabatic unit operating in a TSA (Temperature Swing Absorption) mode or in a combined TSA/PSA (Pressure Swing Absorption) mode. This unit is a finned tube heat exchanger operating alternatively as absorber or desorber (cooled in absorption and heated in desorption) with

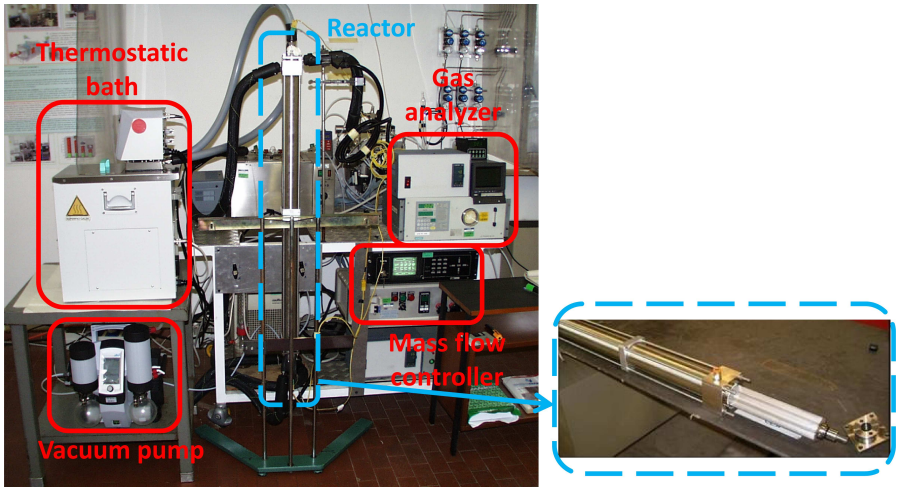


Figure 1: RSE laboratory-scale plant and a detail of the reactor for $CO_2$ absorption/desorption

the sorbent loaded into the free space between the fins. The fixed-bed application needs a small pressure drop (5000 *Pa*); hence the size of the pellets has to be wisely chosen. The best prepared sorbents (DEA on 3 mm alumina spheres) showed a “net $CO_2$ capture" of 50 mg $CO_2$/g of sorbent (5% wt) and a “useful time" of 40 minutes at 40 °C with a sorbent load of 650 g and a gas flow rate of 300 Nl/h (gas composition: 10% $CO_2$, 3% $O_2$, 10% $H_2O$ in $N_2$). The sorbent is completely regenerated by heating the absorption unit up to 85 °C, while depressurizing it and stripping it with a low steam flow. As compared to a conventional $CO_2$ capture process based on a 30 wt% MEA aqueous solution, the proposed process allows to save 35% of the heat required for the sorbent regeneration, so it could be applied on a coal thermal power plant with a 3% energy saving with respect to the MEA aqueous solution process (and with 90% efficiency).

The specific plant we deal with is the experimental equipment, shown in Figures 1 and 2 and described in Section 2, available at the “RSE Processes and catalytic materials" laboratory located in Piacenza (Italy). For a tutorial movie showing the preparation of the sorbent and the assembling of the reactor, the reader is referred to the video available in the RSE website at the address http://www.rse-web.it/video/Impianto-pilota-per-la-cattura-della-CO2.page.

In order to design and study a $CO_2$ capture plant based on this technology, a reliable dynamical model of the capture process and of the subsequent sorbent regeneration is needed. Note that the whole process requires several batch absorption/desorption units (at least four). The model is also

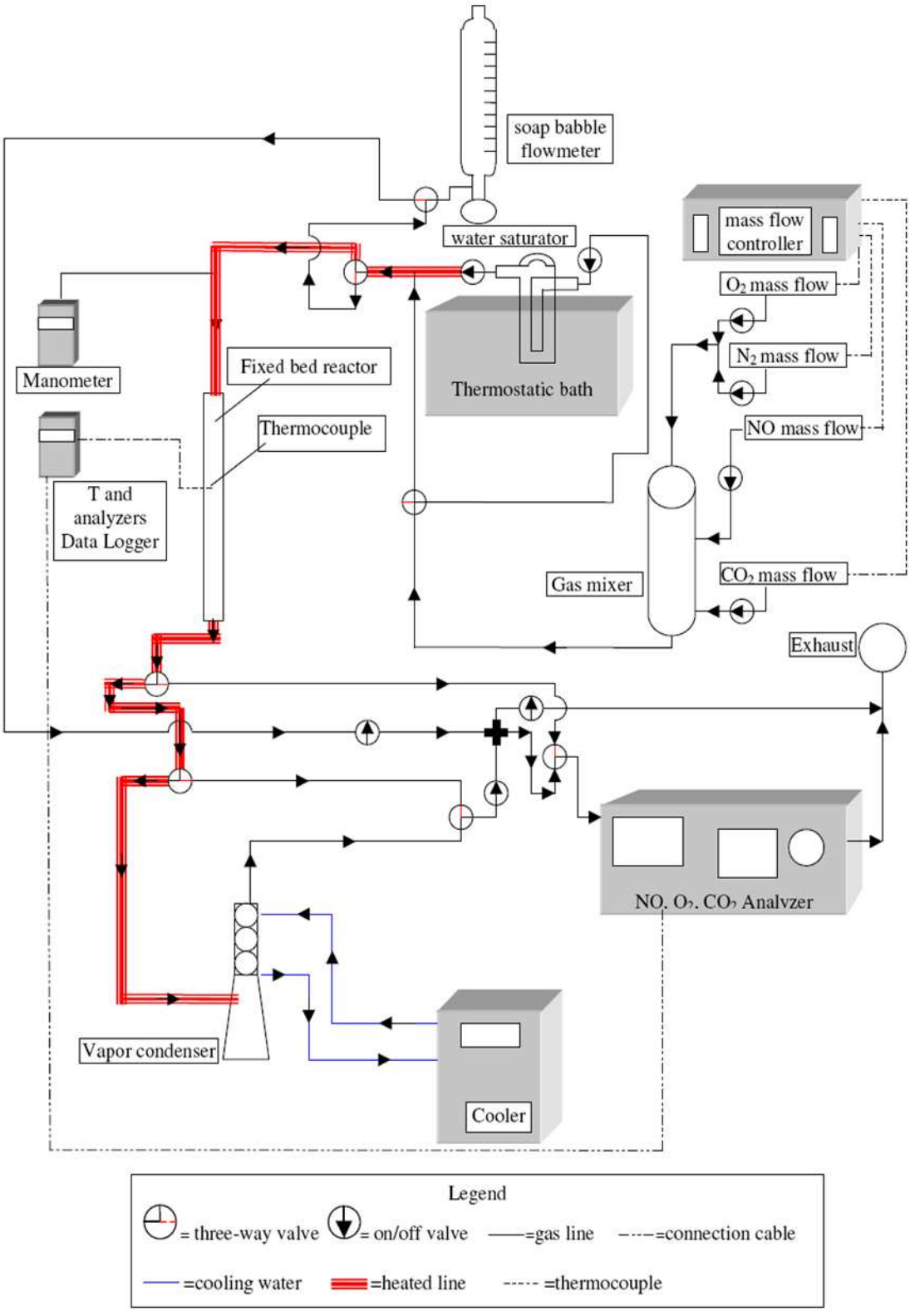


Figure 2: RSE laboratory-scale plant flow chart

useful to design the automation of the coordination of these units.

Our model (Section 2), based on partial differential equations (PDEs), includes the description of gas diffusion inside the porous pellets. By segmenting the reactor into a number of strips and partitioning each pellet into a number of shells, we eventually obtain an Ordinary Differential Equation (ODE) model (Section 3). If, *e.g.*, one considers twenty strips and three shells for each strip, then the final ODE model includes 160 state variables. This model suffers of the uncertainty of the absorption and desorption reaction kinetic parameters. In Section 4, we study the problem of estimating such parameters. The data used for this purpose have been collected in a campaign of experiments performed in the laboratory plant. By means of steady-state data we identify first the ratio of the two parameters; then, by analyzing the transient data, the two parameters can be separately estimated. The obtained model has been validated with fairly satisfactory results. One of the main problems in the industrial use and control of the reactor for $CO_2$ absorption/desorption is the constant wear of the reactor during its life, which may cause the identified model parameters to become obsolete in the long run. We propose then a method to automatically update the estimate of the kinetic parameters.

# 2 Process description

The reference fixed-bed reactor of Figure 1[17] is constituted by a heat exchanger composed of an inner extruded aluminium finned tube, with outer fins extending radially all along its length, and an outer 316 stainless steel tube shell, as schematically outlined in Figure 3. The main geometric and physical characteristics of the reactor are reported in Table 1. The sorbent is made up of highly porous approximately spherical pellets with 36% wt. DEA contents. The sorbent fills the space between the tube and the shell; a porous metallic disk at the bottom of the reactor supports the pellets. A thermal fluid (diathermal oil), supplied by an external refrigerating and heating circulator (see Figure 2), flows into a coil inside the tube, to avoid direct contact with the sorbent, and it heats, or cools, by conduction the sorbent in the cavities between fins. The conductive heat

Table 1: Geometric and physical parameters of the considered reactor

| Symbol = Value | Description |
|---|---|
| $PM_{DEA} = 105 kg/kmol$ | DEA molecular weight |
| $A = 0.9695 \cdot 10^{-3} m^2$ | Reactor cross section area |
| $\Delta p_{tot} = 5000 Pa$ | Overall pressure drop at nominal flow rate |
| $L = 1m$ | Reactor length |
| $M_s = 0.647 kg$ | Sorbent overall mass |
| $p_{ref} = p_0 = 101000 Pa$ | Reference pressure |
| $R_{in} = 0.012 m$ | Reactor inner radius |
| $R_{ex} = 0.0225 m$ | Reactor outer radius |
| $R_0 = 1.5 \cdot 10^{-3} m$ | Sorbent sphere radius |
| $S_r = [2\pi(R_{in} + R_{ex}) + 16 \cdot \cdot (R_{ex} - R_{in})]L = 0.385 m^2$ | Metal-sorbent heat exchange surface (there are 8 fins) |
| $T_{ref} = T_0 = 298 K$ | Reference temperature |
| $\gamma = 43.3 \cdot 10^6 m^2/m^3$ | Active surface per unit volume in sorbent |
| $\varepsilon_s = 0.4$ | Pellet void fraction |
| $\varepsilon_b = 0.4$ | Bulk void fraction |
| $\mu = 0.15 \cdot 10^{-4} Pa \cdot s$ | Gas dynamic viscosity |
| $\rho_s = 680 kg/m^3$ | Pellet mass density |
| $\varphi = 2.4145 \cdot 10^{-8} kmol/m^2$ | Active sites per unit sorbent surface $\left(kmol/m^2\right)$ |
| $w_f = 287 Nl/h$ | Nominal feedgas flow rate |
| $SV = w_f/M_s = 0.45 Nl/(h \cdot g)$ | Space velocity |

exchange with the sorbent is improved by an external jacket where the thermal fluid flow rate from the finned tube outlet can be conveyed (*i.e.* in an ideally series configuration).

The temperature of the fixed-bed sorbent is measured by three type K thermocouples placed respectively at the beginning (point A), at the end (point B) and in the middle (point C) of the sorbent bed. The inlet and the outlet reactor gas composition are measured by continuous analyzers specifically designed for $CO_2$ and recorded by a data logger with 1 Hz sample rate. A vacuum pump depressurizes the reactor during the regeneration carried out as a combination of TSA and PSA modes.

The reactor is schematically represented in Figure 3; the bulk gas flows along the axial coordi-

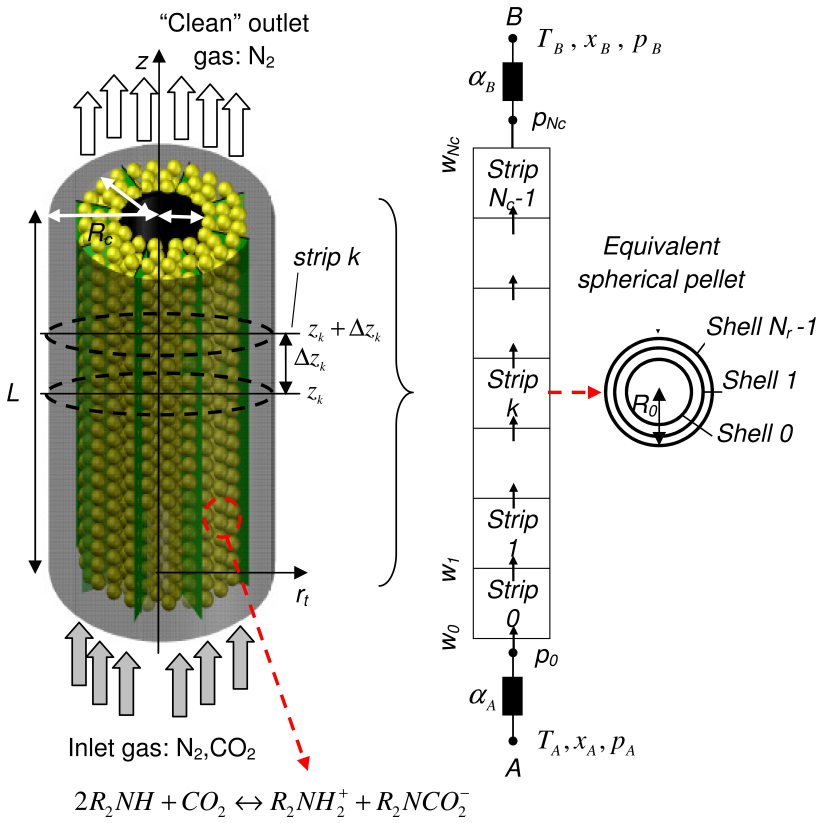


Figure 3: Left: schematic structure of the absorption/desorption reactor; right: reference structure for the reactor model

nate $z$. The pellets are represented as spheres of radius $R_0$. Absorption and desorption occur inside each sphere, as depicted in Figure 4. The overall reaction on the sorbent surface is

$$\underbrace{2R_2NH}_{DEA} + CO_2 \underset{des}{\overset{abs}{\rightleftarrows}} \underbrace{R_2NH_2^+ + R_2NCO_2^-}_{DEA^*}. \tag{1}$$

In the absorption phase, the feedgas mixture reaches the sphere outer surface crossing its limit layer (step 1); then, it flows inside the sphere, into its pores (step 2); once it reaches the surface with the anchored DEA, the exothermal $CO_2$ absorption reaction occurs (step 3); in the desorption phase, the reverse reaction occurs, $CO_2$ is released (step 4) and leaves the pellet (step 5) to reach the bulk flow.

In order to describe the reactor dynamic behaviour, it is necessary to take into account not

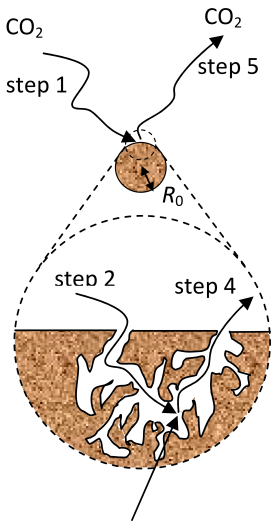


Figure 4: The main steps of the absorption/desorption process inside pellets

only mass and energy exchanges along the gas bulk flow, but also the ones which are due to the absorption/desorption steps and those between gas in the spheres and gas in the bulk region; besides, additional thermal fluxes have to be considered due to the fact that the reactor is a finned tube and that there is the heating/cooling bath to control the sorbent temperature. All these issues are now considered one by one and then described in mathematical form:

- fluid-dynamic and chemical phenomena:
  - mass transport along the reactor bulk, in the gas motion direction (*i.e.* along coordinate *z*): this is essentially due to convection and diffusion along the reactor axial coordinate; diffusion is neglected in the radial direction *r*;
  - mass exchange between the bulk gas and gas inside the pellets, which is due both to convection and to diffusion (in the absorption phase, *e.g.*, $CO_2$ diffuses from the bulk into the pellets, while $N_2$ diffuses towards the bulk);
  - gas motion inside each average spherical pellet, due to diffusion and to convection (along coordinate *R*);
  - momentum transport and friction losses along the bulk gas flow, in the reactor axial

direction;

  - momentum transport and friction losses related to gas flow inside the spherical pellets (along the radial direction $R$ in each sphere);
  - $CO_2$ absorption/desorption mechanisms on the sorbent active surface, inside each sphere; these are strictly related to the reaction chemical kinetics;

- thermal phenomena:
  - heat generation/consumption due to the $CO_2$ absorption/desorption reaction inside the pellets, on their porous surface where the amine is anchored;
  - diffusive heat flux, both in the gas and in the solid sorbent material, along the reactor radial direction $r$;
  - diffusive heat flux in the sorbent material along the reactor longitudinal direction $z$;
  - thermal convective exchange between pellets and bulk gas;
  - thermal convective exchange between pellets and metal (*i.e.* the inner and outer pipes surface and the fins surface);
  - convective energy transport in the bulk gas along the feedgas mixture main motion direction $z$.

To capture all these phenomena, we have developed a two-fold Partial Differential Equation (PDE) model, relating the description of the overall reactor dynamics to a microscopic description of reaction dynamics on the porous pellets inner surface. More precisely, two-dimensional (2-D) conservation equations, with partial derivatives with respect to the reactor longitudinal coordinate $z$ and the reactor radial coordinate $r$, are adopted for the reactor temperature dynamics,[22] as a result of the interaction between the feedgas flow and the absorption/desorption reaction in the porous pellets; this description is complemented with one-dimensional (1-D) conservation equations, with partial derivatives with respect to the pellet radial coordinate $R$, for temperature inside pellets. The dynamics of the chemical variables (molar concentrations and active sites, see Section 2.2.2 and

Santacesaria et al.[23]) and of fluid-dynamic variables (molar flow rates and pressures) are described by 1-D conservation equations (along $z$) for the bulk flow, interacting with 1-D conservation equations (along $R$) inside the pellet particles.

A preliminary congress presentation on our research activity can be found in Bisone et al..[24]

Various models are available in the literature; in some of them, *e.g.* Santacesaria et al.[23]), the bulk flow dynamics are integrated with an *algebraic* description of chemical kinetics inside the pellets, for which different absorption mechanisms (compare Foo and Hameed[25]) have been successfully proposed. In Ruthven's books Ruthven,[26] Ruthven et al.,[27] chemical kinetics as well are treated in a *dynamic* way. In the model proposed herewith, chemical kinetics *dynamics* are described, by making particular reference to the pellet porous surface and taking care of diffusion inside the porous pellets as well; this leads to writing all mass conservation equations inside the pellet spherical volume as distributed-parameter equations.

To properly introduce the equations, we are well advised to make a reference to Table 2, where the adopted list of symbols is displayed. For convenience of notation, for some variables (such as molar densities and molar concentrations) the same symbol will be employed inside the bulk gas and inside the pellet gas, since the reference volume will be specified when introducing each equation.

Table 2: PDE model nomenclature

| Symbol | Description | Unit |
|---|---|---|
| $A$ | reactor cross section area | $m^2$ |
| $A_g$ | cross section area in the gas phase | $m^2$ |
| $\tilde{C}_{CO_2}$ | $CO_2$ molar concentration (in the bulk gas or in the pellet gas) | $kmol/m^3$ |
| $\tilde{C}_{ref}$ | reference molar concentration value | $kmol/m^3$ |
| $\tilde{c}_{pg}$ | gas molar specific heat at constant pressure | $kJ/kmol$ |
| $\tilde{c}_{vg}$ | gas molar specific heat at constant volume | $kJ/kmol$ |

*Table 2: continues in the next page*

*Table 2: continues from previous page*

| Symbol | Description | Unit |
|---|---|---|
| $c_s$ | solid phase mass specific heat | $kJ/kg$ |
| $D_0$ | pellet diameter | $m$ |
| $\mathscr{D}_{CO_2}$ | $CO_2$ axial mass diffusion coefficient | $m^2/s$ |
| $\mathscr{D}_{CO_2,R}$ | $CO_2$ mass radial diffusion coefficient | $m^2/s$ |
| | (along the pellet radius) | |
| $H_s$ | reaction heat | $J/kmol$ |
| $k_{abs}$ | absorption reaction kinetic parameter | $m/s$ |
| $k_{des}$ | desorption reaction kinetic parameter | $m/s$ |
| $k_{fr}$ | friction coefficient in the bulk volume | $kmol/(m^3 s)$ |
| $L$ | reactor length | $m$ |
| $n'''$ | number of pellets per unit volume of the reactor | $m^{-3}$ |
| $PM$ | average molar weight of the bulk gas mixture | $kg/kmol$ |
| $p$ | pressure | $Pa$ |
| $p_{ref}$ | reference pressure value | $Pa$ |
| $R$ | pellet radial coordinate | $m$ |
| $R_0$ | pellet radius | $m$ |
| $R_g$ | universal gas constant | $J/(K \cdot mol)$ |
| $r$ | reactor radius coordinate | $m$ |
| $T_g$ | temperature in the bulk volume gas phase | $K$ |
| $T_{ref}$ | reference temperature value | $K$ |
| $T_s$ | temperature in the bulk volume solid phase | $K$ |
| $u_g$ | bulk gas velocity | $m/s$ |
| $u_R$ | radial gas velocity inside the pellets | $m/s$ |
| $\tilde{w}$ | gas axial molar flow rate along the bulk | $kmol/s$ |

*Table 2: continues in the next page*

*Table 2: continues from previous page*

| Symbol | Description | Unit |
|---|---|---|
| $\tilde{w}'_{conv,s}$ | gas convective molar flow rate per unit length from the bulk towards the pellets outer surface | $kmol/(sm)$ |
| $\tilde{w}'_{CO_2,d}$ | $CO_2$ diffusive molar flow rate per unit length from the bulk towards the pellets outer surface | $kmol/(sm)$ |
| $\tilde{w}'''_{sup}$ | $CO_2$ local molar flow rate, per unit volume, from the gas phase inside the pellet towards the pellet surface | $kmol/(m^3 s)$ |
| $x_{CO_2}$ | $CO_2$ molar fraction (in the bulk gas or in the pellet gas) | $-$ |
| $x_{CO_2,s}$ | $CO_2$ molar fraction on the pellets outer surface | $-$ |
| $z$ | reactor axial coordinate | $m$ |
| $\gamma$ | active surface of a pellet per unit pellet volume | $m^2/m^3$ |
| $\gamma_{sg}$ | heat transfer coefficient between the pellet external surface and the gas in the bulk | $W/(m^2K)$ |
| $\lambda_{s,r}$ | thermal conductivity for the thermal radial diffusive flux in the solid phase | $W/(m^2K)$ |
| $\lambda_{s,z}$ | thermal conductivity for the thermal axial diffusive flux in the solid phase | $W/(m^2K)$ |
| $\varepsilon_g$ | reactor void fraction | $-$ |
| $\varepsilon_p$ | pellet void fraction | $-$ |
| $\theta$ | activated site area fraction | $-$ |
| $\tilde{\rho}$ | gas molar density (in the bulk volume or inside the pellet volume) | $kmol/m^3$ |
| $\rho_s$ | solid phase mass density | $kg/m^3$ |
| $\varphi$ | the *kmol* of DEA sites which can be occupied | $kmol/m^2$ |

*Table 2: continues in the next page*

*Table 2: continues from previous page*

| Symbol | Description | Unit |
|---|---|---|
| | by $CO_2$ in 1 $m^2$ of active surface | |

*Table 2: end*

## 2.1 Bulk equations

### 2.1.1 1-D Mass Conservation Equations

In the reactor bulk volume, two main mass conservation equations are considered: the overall mass conservation equation and $CO_2$ mass conservation equation. Both of them are written in molar form, for convenience.

The overall mass conservation equation, *i.e.* for all gaseous species, can be written as

$$\frac{\partial \tilde{\rho} A_g}{\partial t} + \frac{\partial \tilde{w}}{\partial z} = -\tilde{w}'_{conv,s}, \tag{2}$$

where $A_g$ is the effective cross section area in the gas phase, namely $A_g = A\varepsilon_g$; in turn, $\varepsilon_g$ is the reactor void fraction, *i.e.* $\varepsilon_g$ = (reactor total volume - total solid volume in the reactor)/reactor total volume; $\tilde{w} = \tilde{\rho} A_g u_g$ is the gas axial molar flow rate and $\tilde{\rho} = p/(R_g T_g)$ is the bulk gas molar density. The two terms on the left-hand side are the accumulation and the transport terms along the axial direction $z$ (the bulk flow direction). The term on the right-hand side accounts for the convective mass exchange, in terms of molar flow rate per unit length, between the bulk and the pellets outer surface.

The mass conservation equation for $CO_2$ only reads as

$$\frac{\partial \tilde{C}_{CO_2} A_g}{\partial t} + \frac{\partial \tilde{w} x_{CO_2}}{\partial z} - \frac{\partial}{\partial z}\left( A_g \mathscr{D}_{CO_2} \frac{\partial \tilde{C}_{CO_2}}{\partial z} \right) = -\tilde{w}'_{conv,s} x_{CO_2,s} - \tilde{w}'_{CO_2,d}, \tag{3}$$

where $\tilde{C}_{CO_2}$ and $x_{CO_2}$ are $CO_2$ molar concentration and molar fraction respectively, in the bulk gas; of course, $\tilde{C}_{CO_2} = \tilde{\rho} x_{CO_2}$. $\tilde{w}'_{conv,s}$ is the gas convective molar flow rate, per unit length, towards

the pellets outer surface, while $\tilde{w}'_{CO_2,d}$ is $CO_2$ diffusive molar flow rate, per unit length, towards the pellets outer surface (see Section 2.2.1). The three terms on the left-hand side are the usual $CO_2$ accumulation, transport and diffusion term, respectively, along the axial direction $z$, while the two terms on the right-hand side account for $CO_2$ convective and diffusion motion, in terms of molar flow rate per unit length, between the bulk and the pellets outer surface. As for the diffusion coefficient $\mathscr{D}_{CO_2}$, we have assumed the classical binary diffusion of $CO_2$ in $N_2$.

### 2.1.2 Linear Momentum Conservation Equation

Momentum conservation equation in the bulk volume can be written as

$$\frac{\partial \tilde{w}}{\partial t} + \frac{\partial A_g \tilde{\rho} u^2}{\partial z} + A_g \frac{\partial p}{\partial z} + k_{fr} \frac{\tilde{w}}{\tilde{\rho}} = 0, \tag{4}$$

where, from left to right, the usual accumulation, transport, pressure and friction terms appear. The friction coefficient $k_{fr}$ can be expressed as the combination of a "laminar" and a "turbulent" term (see the Ergun correlation in Bird et al.[28] and in Froment and Bischoff[29])

$$k_{fr} = k_l + k_s |\tilde{w}|, \tag{5}$$

with

$$k_l = 150 \frac{(1-\varepsilon_g)^2}{\varepsilon_g^2} \frac{\mu}{D_0^2}$$

$$k_s = 1.75 \frac{1-\varepsilon_g}{\varepsilon_g^2} \frac{PM}{D_0^2 A}$$

where, we remind, $\varepsilon_g$ is the bulk void fraction and $D_0$ the pellet diameter, while $PM$ is the average molar weight of the gas mixture.

### 2.1.3 Energy Conservation Equations

In the bulk volume, again, two main energy conservation equations are taken into account, for the gas phase and for the solid phase respectively.

Energy conservation for the gas phase can be written as

$$\frac{\partial 2\pi r\tilde{\rho}\tilde{c}_{vg}T_g}{\partial t}+\tilde{w}_g''2\pi r\tilde{c}_{pg}\frac{\partial T_g}{\partial z}=2\pi rn'''4\pi R_0^2\gamma_{sg}\left(T_s-T_g\right), \tag{6}$$

where $T_g$ is the gas phase temperature, $c_{vg}$ and $c_{pg}$ the gas molar specific heat at constant volume and at constant pressure respectively, $\tilde{w}_g''=\tilde{w}/A_g$ and $\gamma_{sg}$ is the heat transfer coefficient between the pellet external surface and the gas in the bulk. The terms on left-hand side describe energy accumulation and convective transport along the axial direction $z$, while the term on the right-hand side accounts for heat exchange between the gas phase and the solid phase. Indeed, $T_s$ is the solid phase temperature, while $n'''$ is the number of pellets per unit volume of the reactor (we remind that the ideal average pellet is assumed as a sphere of radius $R_0$). Diffusion along the reactor axial direction $z$ has not been included, since it is negligible with respect to the convective transport term. Diffusion along the reactor radial direction $r$ has not been included explicitly in this equation, because it is accounted for by the thermal conductivity and heat exchange coefficient in the solid phase energy conservation equation (see Froment and Bischoff[29] and parameter $\lambda_s$ in (7)).

Energy conservation equation of the solid phase (2-D) can be written as

$$\frac{\partial 2\pi r\rho_s c_s T_s}{\partial t}+\frac{\partial}{\partial r}\left(2\pi r\lambda_{s,r}\frac{\partial T_s}{\partial r}\right)+\frac{\partial}{\partial z}\left(2\pi r\lambda_{s,z}\frac{\partial T_s}{\partial z}\right)=E_s2\pi r-2\pi rn'''4\pi R_0^2\gamma_{sg}\left(T_s-T_g\right), \tag{7}$$

where $T_s$ is the solid phase temperature, while $\rho_s$ and $c_s$ the solid phase mass density and specific heat respectively. The terms on left-hand side describe energy accumulation (in the solid phase), diffusion along the reactor radial direction $r$ and along the reactor axial direction $z$, while the terms on the right-hand side account for the absorption/desorption reaction energy generation/consumption and, as in the previous equation, for heat exchange between the solid phase and the gas phase. The heat transfer coefficient $\gamma_{sg}$, between the pellet surface and the gas phase, has been evaluated here by a Colburn formula[30] where the Nusselt number of the particles is related to the Reynolds number of the particles and the Prandtl number of the fluid. The radial diffusive

thermal flux has been considered for the solid phase only, as already remarked; obviously, the correlation (Froment and Bischoff,[29] Section 11.7, and Balakrishnan and Pei[30]) adopted for thermal conductivity $\lambda_{s,r}$ in the radial direction accounts for the presence not only of the solid phase but also of the gas phase. The axial diffusive thermal flux, instead, regards the solid phase only, with its thermal conductivity $\lambda_{s,z}$, which has been computed in a simple way as the product of alumina conductivity and the factor $(1-\varepsilon_g)$.

$E_s 2\pi r$ is the power flux ($W/m^2$) released/absorbed by the $CO_2$ absorption/desorption reaction on the pellet porous inner surface, *i.e.* the product of the reaction heat $H_s$ and of the reacting moles:

$$E_s = \int_0^{R_0} 4\pi R^2 \gamma H_s n''' \left[k_{abs}(1-\theta)\tilde{C}_{CO_2} - k_{des}\theta\tilde{C}_{ref}\right] dR, \tag{8}$$

where $R_0$ is the pellet radius, $\gamma$ the active surface of a pellet per unit pellet volume, and $\theta$ the inner area fraction occupied by absorbed $CO_2$ molecules; $k_{abs}$ and $k_{des}$ are absorption and desorption coefficients describing the reaction kinetics (see Section 2.2.2).

## 2.2 Conservation equations in the pellet volume

### 2.2.1 1-D Mass Conservation Equations

In the pellet volume, two main mass conservation equations are considered: the overall mass conservation equation and $CO_2$ mass conservation equation, as in the bulk volume. Again, both of them are written in molar form, for convenience.

Mass conservation equation for all species in the gas phase inside pellets can be written as

$$\frac{\partial}{\partial t}\left(4\pi R^2 \varepsilon_p \tilde{\rho}\right) + \frac{\partial}{\partial R}\left(4\pi R^2 \varepsilon_p \tilde{\rho} u_R\right) = -4\pi R^2 \tilde{w}'''_{sup}, \tag{9}$$

where $\varepsilon_p$ is the pellet void fraction, $u_R$ the gas velocity inside pellets and $\tilde{w}'''_{sup}$ the molar flow rate, per unit volume, between the gas phase inside the pellet and the pellet surface (due to $CO_2$ absorption/desorption, see Section 2.2.2). The terms on the left-hand side account for accumulation

and for radial transport respectively. Notice that $\tilde{\rho}$, namely gas molar density inside pellets, is computed at temperature $T_s$.

Mass conservation equation for $CO_2$ inside the pellets reads as

$$\frac{\partial}{\partial t}\left(4\pi R^2 \varepsilon_p \tilde{C}_{CO_2}\right) + \frac{\partial}{\partial R}\left(4\pi R^2 \varepsilon_p \tilde{\rho} u_R x_{CO_2}\right) - \frac{\partial}{\partial R}\left(4\pi R^2 \mathscr{D}_{CO_2,R} \varepsilon_p \frac{\partial \tilde{C}_{CO_2}}{\partial R}\right) = -4\pi R^2 \tilde{w}'''_{sup}, \quad (10)$$

with the accumulation term, the radial transport term and the radial diffusion term on the left-hand side; notice that $\tilde{C}_{CO_2} \equiv \tilde{C}_{CO_2}(R,z,t)$ and $x_{CO_2} \equiv x_{CO_2}(R,z,t)$ are $CO_2$ molar concentration and molar fraction, respectively, in the gas phase inside pellets.

As for parameter $\mathscr{D}_{CO_2,R}$, *i.e.* $CO_2$ mass radial diffusion coefficient, describing diffusion inside the porous pellet, a simple correlation based on the "dusty-gas" model has been adopted,[31] taking into account inner porosity (the ratio of the pores volume and the particle volume), inner surface per unit mass, Knudsen diffusivity (which is related to tortuosity for instance) and binary diffusion.

Subtracting (10) from (9) side by side and assuming that $\partial \tilde{C}_{CO_2} = \tilde{\rho}\,\partial x_{CO_2}$ (based on the further assumption that pressure and temperature are uniform in the gas phase inside the pellet) yields

$$\frac{\partial}{\partial t}\left[4\pi R^2 \varepsilon_p \tilde{\rho}\left(1 - x_{CO_2}\right)\right] + \frac{\partial}{\partial R}\left[4\pi R^2 \varepsilon_p \tilde{\rho} u_R \left(1 - x_{CO_2}\right)\right] + \frac{\partial}{\partial R}\left(4\pi R^2 \mathscr{D}_{CO_2,R} \varepsilon_p \tilde{\rho} \frac{\partial x_{CO_2}}{\partial R}\right) = 0. \quad (11)$$

Thus, integrating both sides, with respect to $R$, between 0 and $R$, one obtains

$$\frac{\partial}{\partial t}\int_0^R \left[4\pi \xi^2 \varepsilon_p \tilde{\rho}\left(1 - x_{CO_2}\right)\right] d\xi + 4\pi R^2 \varepsilon_p \tilde{\rho}\left[u_R\left(1 - x_{CO_2}\right) + \mathscr{D}_{CO_2,R}\frac{\partial x_{CO_2}}{\partial R}\right] = 0. \quad (12)$$

Therefore,

$$u_R = -\frac{1}{1 - x_{CO_2}}\left[\mathscr{D}_{CO_2,R}\frac{\partial x_{CO_2}}{\partial R} + \frac{1}{4\pi R^2 \varepsilon_p \tilde{\rho}}\frac{\partial}{\partial t}\int_0^R \left[4\pi \xi^2 \varepsilon_p \tilde{\rho}\left(1 - x_{CO_2}\right)\right] d\xi\right]. \quad (13)$$

Now, replacing this expression in (10) gives

$$\frac{\partial}{\partial t}\left(4\pi R^2 \varepsilon_p \tilde{\rho} x_{CO_2}\right) - \frac{\partial}{\partial R}\left(4\pi R^2 \varepsilon_p \tilde{\rho} \frac{\mathscr{D}_{CO_2,R}}{1-x_{CO_2}} \frac{\partial x_{CO_2}}{\partial R}\right) + \\ - \frac{\partial}{\partial R}\left(\frac{x_{CO_2}}{1-x_{CO_2}} \frac{\partial}{\partial t} \int_0^R \left[4\pi \xi^2 \varepsilon_p \tilde{\rho}\left(1-x_{CO_2}\right)\right] d\xi\right) = -4\pi R^2 \tilde{w}'''_{sup}. \quad (14)$$

The related boundary condition accounts for $CO_2$ mass transfer between the bulk and the pellet gas, due to $CO_2$ convective and diffusive flux on the pellet surface, *i.e.* for $R = R_0$. Remind that $x_{CO_2,s}$ (see (3), in Section 2.1.1) is the $CO_2$ molar fraction on the pellet surface, namely $x_{CO_2}|_{R=R_0}$. The $CO_2$ convective molar flow rate on the pellet surface can be written as

$$\tilde{w}_{conv,s} x_{CO_2,s} = 4\pi R_0^2 \varepsilon_p \left(\tilde{\rho} u_R x_{CO_2}\right)|_{R=R_0} = -4\pi R_0^2 \varepsilon_p \mathscr{D}_{CO_2,R} \tilde{\rho} \left(\frac{x_{CO_2}}{1-x_{CO_2}} \frac{\partial x_{CO_2}}{\partial R}\right)\Bigg|_{R=R_0} = \\ = -4\pi R_0^2 \varepsilon_p \mathscr{D}_{CO_2,R} \tilde{\rho} \frac{x_{CO_2,s}}{1-x_{CO_2,s}} \left(\frac{\partial x_{CO_2}}{\partial R}\right)\Bigg|_{R=R_0} \quad (15)$$

and $CO_2$ diffusive molar flow rate as

$$\tilde{w}_{CO_2,d} = 4\pi R_0^2 \varepsilon_p \mathscr{D}_{CO_2,R} \tilde{\rho} \left(\frac{\partial x_{CO_2}}{\partial R}\right)\Bigg|_{R_0}; \quad (16)$$

therefore, the boundary condition reads

$$4\pi R_0^2 h_{CO_2}\left(x_{CO_2,bulk} - x_{CO_2,s}\right) = 4\pi R_0^2 \mathscr{D}_{CO_2,R} \tilde{\rho} \frac{1}{1-x_{CO_2,s}} \left(\frac{\partial x_{CO_2}}{\partial R}\right)\Bigg|_{R=R_0}, \quad (17)$$

where $h_{CO_2}$ is a suitable $CO_2$ mass (molar) transfer coefficient.

Of course, $CO_2$ convective and diffusive molar flow rates per unit length on the right-hand side of (3), namely $\tilde{w}'_{conv,s} x_{CO_2,s}$ and $\tilde{w}'_{CO_2,d}$, are related to the just computed $CO_2$ convective and diffusive molar flow rates on the pellet surface by the pellet density per unit length $N_p/L$, where

$N_p$ is the number of pellets in the reactor and $L$ is the reactor length:

$$\tilde{w}'_{conv,s} x_{CO_2,s} = \tilde{w}_{conv,s} x_{CO_2,s} \frac{N_p}{L} \tag{18}$$

$$\tilde{w}'_{CO_2,d} = \tilde{w}_{CO_2,d} \frac{N_p}{L} \tag{19}$$

Finally, we remark that, in case $x_{CO_2} \to 1$, *i.e.* in case there is $CO_2$ only in the gas mixture (as it happens in the desorbing stage of the overall process), then there is no $CO_2$ diffusion, so equation (10) disappears from the model, while equation (9) still holds.

### 2.2.2 Chemical kinetics

The Langmuir theory[29] (compare also Serna-Guerrero and Sayari,[32] for a discussion of different approaches to kinetic dynamics) can be employed to describe $CO_2$ absorption and desorption into the sorbent. Let $\theta$ be the area fraction occupied by $CO_2$ molecules tied to the DEA on the porous medium surface, $\tilde{C}_{CO_2}$ $CO_2$ molar concentration, in the gas phase, in the porous medium, $T_s$ the sorbent temperature (assumed as uniform along $R$), $\varphi$ the *kmol* of DEA sites which can be occupied by $CO_2$ in 1 $m^2$ of active surface. Then, reaction kinetics can be described by the conservation equation

$$\varphi \frac{\partial \theta(z,r,R,t)}{\partial t} = k_{abs}(T_s(z,r,t)) \cdot \tilde{C}_{CO_2}(z,r,R,t) \cdot (1 - \theta(z,r,R,t)) + \\ - k_{des}(T_s(z,r,t)) \tilde{C}_{ref} \theta(z,r,R,t). \tag{20}$$

where the reference molar concentration is $\tilde{C}_{ref} = p_{ref}/(R_g T_{ref})$ (the reference pressure and temperature, here, are assumed as the standard conditions values, *i.e.* $p_{ref} = 101000Pa$ and $T_{ref} = 298K$). $k_{abs}$ and $k_{des}$ are, respectively, the absorption and desorption kinetic parameters in the reaction between $CO_2$ and DEA sites.

The $CO_2$ molar flow rate per unit volume $\tilde{w}'''_{sup}$ in (9) and (10) is, of course, directly related to

the reaction kinetic equation (20):

$$\tilde{w}'''_{sup} = \gamma \left[ k_{abs}(T_s(z,r,t)) \tilde{C}_{CO_2}(z,r,R,t) \left(1 - \theta(z,r,R,t)\right) - k_{des}(T_s(z,r,t)) \tilde{C}_{ref} \theta(z,r,R,t) \right], \quad (21)$$

where $\gamma$ is defined as the ratio of the total surface, inside pellets, where there are active sites and the volume of the pellets.

$k_{abs}$ and $k_{des}$ are the main uncertain parameters in the model. The problem of their identification will be addressed in Section 4.

### 2.2.3 Momentum Conservation Equation Inside the Pellet

In principle, the model would require a momentum conservation equation in the pellet as well:

$$\frac{\partial}{\partial t}\left(4\pi R^2 \tilde{\rho} u_R\right) + \frac{\partial}{\partial R}\left(4\pi R^2 \tilde{\rho} u_R^2\right) + 4\pi R^2 \frac{\partial p}{\partial R} - 4\pi R^2 k_{fr,p} \rho u_R = 0, \quad (22)$$

where, from left to right, the usual accumulation, transport (along the radial coordinate $R$ inside the pellets), pressure and friction terms appear.

However, for simplicity, here we have assumed that the pressure is uniform inside the pellet and equal to the bulk pressure. Further inquiries on this approximation are currently underway.

# 3 Finite-dimensional model

By means of a finite-volume approach, we have derived an Ordinary Differential Equation (ODE) model (Table 3) from the PDE model of the previous section.

In few words, the reactor length $L$ is divided into $N_c$ strips (see Figure 3), in each of which the bulk gas behaviour is described by ordinary differential mass, energy and momentum conservation equations, obtained by integrating the PDEs just described along the spatial coordinate $z$ first, along the bulk gas flow direction, and then along the radial coordinate $r$. The process variables in the generic $k$-th strip, $\Delta z_k$ long, between $z_k$ and $z_{k+1}$, are defined by their average value along $z$

between $z_k$ and $z_{k+1}$. For convective fluxes of energy and mass an upstream formulation has been adopted. Momentum conservation equations have been integrated in staggered cells with respect to the mass and energy conservation equations, so they are employed to define the molar flow rates at the junctions between adjacent strips. For simplicity, all strips are assumed as identical width: $\Delta z_k = \Delta z = L/N_c$, $\forall k = 0,\ldots,N_c-1$.

Similarly, an average equivalent spherical pellet, of radius $R_0$, is divided into $N_r$ spherical shell volumes and ordinary differential mass conservation equations and chemical kinetics equations are considered in each *i*-th shell, $i = 0,\ldots,N_r-1$. Here, all shells are assumed as the same volume $V_g = 4\pi {R_0}^3/(3N_r)$. In the conservation equations for the bulk region, the "effect" of a single pellet is multiplied by the average number of pellets in a strip, i.e. $N_p\Delta z/L$, with $N_p$ the total number of pellets in the reactor.

Integration along the reactor radial coordinate *r* allows to write energy conservation equations in the sorbent with reference to a sorbent average temperature $T_k$ in each strip *k*.

One can verify that the momentum and mass accumulation terms in the bulk gas volume, namely the terms related to pressure and flow rate wave propagation, have very small time-scale dynamics, so they give rise to stiff equations; therefore, the quasi-steady state assumption has been made. The same assumption is valid for the momentum conservation equations in the porous pellet volume; moreover, radial convective flow in the pellets is very small, indeed it is zero at steady state, so pressure inside the pellet has been assumed to coincide with the fluid pressure in the bulk region adjacent to the pellet (in other words, the friction term in the radial momentum conservation equations has been neglected).

Hydrodynamic boundary conditions for the reactor inlet and/or outlet have been set as (see the two black boxes at the top and bottom of the reactor, in Figure 3)

$$\sigma_A w_b(0,t) = \alpha_A\left(p_A(t) - p_0(t)\right) + \sigma_A w_A(t) \tag{23}$$

$$\sigma_B w_b(N_c,t) = \alpha_B\left(p_1(t) - p_B(t)\right) - \sigma_B w_B(t), \tag{24}$$

where $w_b(0,t)$ and $w_b(N_c,t)$ are the reactor inlet and outlet molar flow rates, $p_0$ and $p_1$ are the inlet and outlet pressures, $\sigma_A$, $\sigma_B$, $\alpha_A$ and $\alpha_B$ are suitable coefficients. For instance,

- for $\{\sigma_A = 1, \alpha_A = 0, \sigma_B = 0, \alpha_B = 1\}$, the reactor outlet pressure is set as $p_1(t) = p_B(t)$ and the injected inlet flow rate is $w_b(0,t) = w_A(t)$, where $p_B(t)$ and $w_A(t)$ are an assigned pressure and flow rate, respectively;
- for $\{\sigma_A = 1, \alpha_A = 0, w_A = 0, \sigma_B = 0, \alpha_B = 1\}$, one has $p_1(t) = p_B(t)$ and $w_b(0,t) = 0$, as in the heating phase while $CO_2$ exits through terminal B.

Boundary conditions for bulk energy conservation equations are expressed by means of temperatures $T_A$ and $T_B$ and of $CO_2$ molar fractions $x_A$ and $x_B$. For instance, if $w_b(0,t) \geq 0$, at point A there are an entering $CO_2$ molar flow rate $w_b(0,t)x_A(t)$ and entering convective power $w_b(0,t)C_p(T_A)T_A(t)$; if $w_b(0,t) < 0$, instead, $x_A$ and $T_A$, and therefore the exiting molar flow rate and the exiting convective power are computed by the model. Similar considerations can be drawn at point B for flow rate $w_b(N_c,t)$: if $w_b(N_c,t) < 0$, for instance, there are molar flow rate and convective power flow entering B, and their values are determined by $x_B$ and $T_B$.

The obtained overall model includes $N = 2N_c(N_r + 1)$ state equations (with our choice $N_c = 20$ and $N_r = 3$, 160 state equations). It also includes a number of algebraic equations. The model has been implemented by a stand-alone C codex, which can be easily connected industrial plant simulators; besides, it is useful for identification purposes, as described in the subsequent sections.

# 4 Kinetic parameters identification via bench experiments

The ODE version of the kinetics equation (20) is

$$\varphi \dot{\theta}_{k,i}(t) = k_{abs}\left(T_{s,k}(t)\right) \cdot \left(1 - \theta_{k,i}(t)\right) \cdot \tilde{C}_{k,i}(t) - k_{des}\left(T_{s,k}(t)\right) \cdot \tilde{C}_{ref} \cdot \theta_{k,i}(t), \tag{25}$$

where $i$ is the shell index and $k$ the strip index. The main uncertain parameters are the absorption and desorption kinetic coefficients $k_{abs}$ and $k_{des}$, which strongly depend on temperature in the

Table 3: ODE model synopsis (CE = Conservation Equation)

| **Chemical kinetics** |
|---|
| *Active site CE, for* $i = 1,\ldots,N_r,\ k = 0,\ldots,N_c-1$*:* |
| - $CO_2$ absorption and desorption into the pellet (see (25)). |
| **Hydrodynamic equations** |
| *Global mass CE in the pellet, for* $i = 1,\ldots,N_r$, $k = 0,\ldots,N_c-1$ : |
| - quasi-steady state conditions; |
| - no convective flow rate at the sphere centre; |
| - bulk-sorbent boundary flow rate due to absorption from all shells; |
| *Global mass CE along the bulk flow, for* $k = 0,\ldots,N_c-1$ : |
| - no accumulation (quasi-stationary assumption for $p$ and $T$). |
| *Momentum CE in the bulk region, for* $k = 0,\ldots,N_c$ : |
| - quasi-steady state conditions; |
| - laminar friction only. |
| **Mass conservation equations** |
| *$CO_2$ mass CE in the pellet volume, for* $i = 0,\ldots,N_r-1$, $k = 0,\ldots,N_c-1$ : |
| - $CO_2$ accumulation; |
| - $CO_2$ absorption/desorption; |
| - $CO_2$ radial diffusion, to/from the adjacent shells; |
| - $CO_2$ radial convection, to/from the adjacent shells. |
| *$CO_2$ mass CE in the bulk volume, for* $k = 0,\ldots,N_c-1$ : |
| - $CO_2$ accumulation; |
| - $CO_2$ convective and diffusive mass exchange with the pellet surface; |
| - $CO_2$ bulk axial diffusion, to/from the adjacent strips; |
| - $CO_2$ bulk axial convection, to/from the adjacent strips. |
| **Energy conservation equations** |
| *Energy CE in the sorbent volume, for* $k = 0,\ldots,N_c-1$ : |
| - energy accumulation; |
| - conduction in the reactor axial direction, to/from the adjacent strips; |
| - absorption/desorption reaction heat; |
| - heat exchange between the pellets and the bulk gas; |
| - heat exchange between the pellets and the exchanger metal surface. |
| *Energy CEs in the bulk volume, for* $k = 0,\ldots,N_c-1$ : |
| - accumulation is neglected in the bulk gas; |
| - heat exchange between the pellets and the bulk gas; |
| - energy axial transport to/from the adjacent strips, by bulk flow rate; |
| - energy axial conduction, to/from the adjacent strips. |

porous medium.

The identification procedure is based on data collected in twelve *ad hoc* dynamic experiments

carried out on the test rig. Each experiment started from completely regenerated sorbent. Absorption was carried out by feeding the reactor with $N_2$, steam (10% molar fraction) and $CO_2$ mixtures with fixed $CO_2$ concentrations, setting the inlet gas flow rates by means of the mass-flow controllers ($w_f$ = 219 Nl/h was the total feedgas flow rate), and keeping the reactor temperature constant and uniform by using the external circulator. Three different inlet mixtures (with $CO_2$ molar fraction equal to 0.05, 0.10 and 0.25) and four temperatures (25 °C, 40 °C, 60 °C and 85 °C) have been considered: this way, we have collected twelve sequences of data, each one corresponding to a pair (molar fraction, temperature), with sample rate 1 Hz. In each test, the $CO_2$ molar fraction at the reactor outlet $x_{CO_2 out}$ was measured, up to the final steady state of complete sorbent saturation ($\theta = 1$ in (25)). As for the temperature $T_{s,k}$, we have used the values provided by our model; notice in passing that, in the reactor sections where the three thermocouples are placed (beginning, middle, end), the temperature supplied by the model is in fair agreement with the measured temperature.

The adopted estimation procedure can be summarized as follows:

1. *identification of the ratio $\eta := k_{abs}/k_{des}$ via steady-state data.*

   By means of the measurements of $x_{CO_2 out}$, it has been possible to evaluate the steady-state value of the amount of adsorbed $CO_2$ in each test, namely $\Gamma$ (kmol). The corresponding twelve points are depicted in Figure 5. The obtained values for $\Gamma$ have been employed to evaluate (pointwise) the twelve values of the ratio $\eta := k_{abs}/k_{des}$. They have also allowed the evaluation of the standard enthalpy variation of reaction (1), which, in turn, has allowed the determination of $\eta$ as a function of the temperature.

2. *Identification of $k_{abs}$ and $k_{des}$ via transient data.*

   The values of $\eta$ identified as indicated in the previous point, together with *transient* data gathered from the experiments have been used to identify $k_{abs}$ and $k_{des}$ separately (as functions of the temperature). In this phase, we have used three of the twelve experiments only, precisely those carried out with inlet $CO_2$ molar fraction equal to 0.1 and at 40 °C, 60 °C and 85 °C temperature.

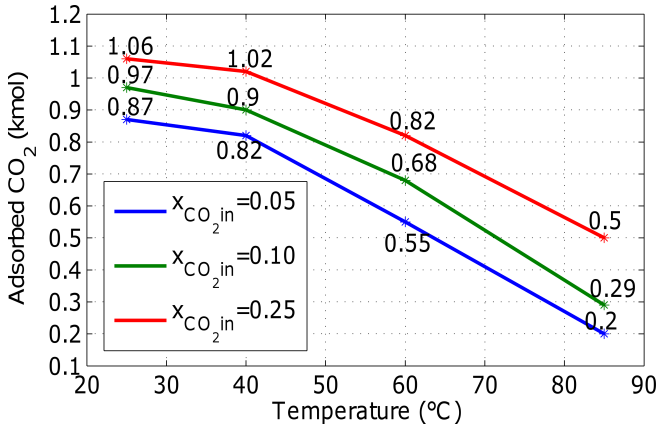


Figure 5: Amount $\Gamma$ of absorbed $CO_2$ (*kmol*) at steady state: experimental results as functions of temperature, for different $CO_2$ inlet molar fractions

This way, the identification procedure has been completed and a fully specified model has been tuned (including the dependence of parameters $k_{abs}$ and $k_{des}$ upon the sorbent temperature).

3. *Validation of the identified model via transient data*.

   The remaining sequences of experimental data have been used for validation purposes, namely the simulations provided by our model have been compared to such data, with satisfactory agreement.

In the sequel, each of these steps is elaborated in detail.

Note that in the equations the temperature is assumed to be expressed in Kelvin, whereas in the drawings it is expressed in Celsius.

## 4.1 Step 1: identification from steady-state data

We now address the issue of estimating $\eta := k_{abs}/k_{des}$. To this purpose we rely on the amount $\Gamma$ of absorbed $CO_2$ in steady state obtained in each of the twelve experimental tests described above and reported in Figure 5. In each test, of course, the outlet $CO_2$ molar fraction equals the inlet one, at steady state. As one can notice from the figure, keeping the inlet concentration constant yields an increasing $\Gamma$ as temperature decreases.

### 4.1.1 Pointwise estimation of $\eta$

Recall kinetic equation (25). Here, three basic unknowns appear: $\varphi$, $k_{abs}$ and $k_{des}$. Parameter $\varphi$ is considered as an unknown constant; on the contrary, the dependence of $k_{abs}$ and $k_{des}$ upon the temperature cannot be neglected. In this respect, observe that, in steady-state conditions, temperature is uniform in the porous medium, so $T_{s,k} = const = T$.

At steady state (saturation condition), the $CO_2$ molar fraction in each surface element in all pellets has to equal the inlet $CO_2$ molar fraction $x_{CO_2 in}$; therefore, letting $\theta_\infty$ be the uniform steady-state area fraction occupied by DEA tied to $CO_2$, one has, from (25), that

$$\theta_\infty = \frac{\eta x_{CO_2 in}}{\eta x_{CO_2 in} + T/T_0}, \tag{26}$$

where the gas pressure is assumed as uniform and equal to the standard conditions pressure.

Now, in the $i$-th experiment, the absorbed $CO_2$ amount is

$$(\Gamma)_i = \varphi \cdot (M_s \gamma/\rho_s) \cdot (\theta_\infty)_i; \tag{27}$$

therefore, since (26) yields, at least formally, that $\theta_\infty \to 1$ for $T \to 0$, from (27) one can deduce that $\Gamma$ tends to a limit value

$$\Gamma_{limit} = \varphi \cdot (M_s \gamma/\rho_s) \tag{28}$$

so that

$$(\Gamma)_i/\Gamma_{limit} = (\theta_\infty)_i. \tag{29}$$

Therefore, if $\Gamma_{limit}$ is assigned and the number of occupied kmols $(\Gamma)_i$ in each $i$-th experiment is measured, then (29) gives the occupied site fraction $(\theta_\infty)_i$ and (26) the corresponding value of $(\eta)_i$:

$$(\eta)_i = \frac{(\theta_\infty)_i}{1-(\theta_\infty)_i} \frac{1}{(x_{CO_2 in})_i} \frac{(T)_i}{T_0} \tag{30}$$

For the twelve performed experiments, the $(\eta)_i$ values obtained for $\Gamma_{limit}$ = 1.1, for instance, are

collected in Table 4, together with their mean values $\bar{\eta}$ with respect to the $CO_2$ inlet molar fraction, obtained for each of the four considered temperatures. Obviously, $\bar{\eta}$ is temperature-dependent: $\bar{\eta} = \bar{\eta}(T)$). Parameter $\varphi$, in turn, can be identified from (28).

In order to best identify $\Gamma_{limit}$, the following iterative optimization procedure is proposed:

1. set a tentative value for $\Gamma_{limit}$;
2. thanks to the available tests, determine $\bar{\eta}(T)$ and $\varphi$ from $\Gamma_{limit}$;
3. for each experiment $i$, compute $(\theta_\infty)_i$ from (26) and therefore $(\Gamma_{model})_i$ from (27);
4. compute the mean square error MSE, or the standard deviation SD, between the experimental values $(\Gamma_{exper})_i$ and the computed values $(\Gamma_{model})_i$;
5. find the value for $\Gamma_{limit}$ minimizing MSE or SD.

A simple way to accomplish step 5 is to explore a sufficiently wide interval of discrete values for $\Gamma_{limit}$. For the set of tests under study, Table 5 reports the computed values of MSE and SD for different choices of $\Gamma_{limit}$. MSE appears to be minimized by $\Gamma_{limit}$ = 1.09: the related values of $\bar{\eta}(T)$ are reported in Table 6, while (28) yields $\varphi = \Gamma_{limit}/(\gamma M_s/\rho_s) = 2.4145 \cdot 10^{-8}$ kmol/m$^2$.

Comparison between Table 4 and Table 6 highlights the influence of $\Gamma_{limit}$ on $\bar{\eta}(T)$. Finally, one can remark that the assumption of a unique $\Gamma_{limit}$ for $T \to 0$, which is not straightforward from (26), is justified by the fact that, if $\Gamma_{limit}$ depended on $x_{CO_2}$, then $\eta$ should be a function of $x_{CO_2}$, which is not plausible from the definition of $\eta$.

The next section highlights the relation between parameter $\theta$, or $\bar{\eta}(T)$, and the equilibrium constant $K_{eq}(T)$ of the reaction between DEA and $CO_2$, thus enabling the evaluation of the standard enthalpy of that reaction.

Table 4: Values of $\eta$ at experimental temperatures and concentrations, and mean values $\bar{\eta}$, for $\Gamma_{limit} = 1.1$

| | $x_1 = 0.05$ | $x_2 = 0.10$ | $x_3 = 0.25$ | $\bar{\eta}$ |
|---|---|---|---|---|
| $T_0 = 25$ °C | 75.648 | 74.602 | 105.890 | 85.380 |
| $T_1 = 40$ °C | 61.520 | 47.265 | 53.567 | 54.117 |
| $T_2 = 60$ °C | 22.349 | 18.092 | 13.090 | 17.844 |
| $T_3 = 85$ °C | 5.339 | 4.301 | 4.004 | 4.548 |

Table 5: MSE and SD for some values of $\Gamma_{limit}$

| $\Gamma_{limit}$ | Mean Square Error | Standard Deviation |
|---|---|---|
| 1.15 | 0.232 | 0.0211 |
| 1.10 | 0.208 | 0.0190 |
| 1.09 | 0.207 | 0.0188 |
| 1.08 | 0.218 | 0.0198 |
| 1.05 | 0.690 | 0.0627 |

Table 6: Experimental values of $\eta$ and computed $\bar{\eta}$ for $\Gamma_{limit} = 1.09$

| | $x_1 = 0.05$ | $x_2 = 0.10$ | $x_3 = 0.25$ | $\bar{\eta}$ |
|---|---|---|---|---|
| $T_0 = 25$ °C | 79.091 | 80.833 | 141.333 | 100.419 |
| $T_1 = 40$ °C | 63.798 | 49.753 | 61.220 | 58.257 |
| $T_2 = 60$ °C | 22.763 | 18.533 | 13.575 | 18.290 |
| $T_3 = 85$ °C | 5.399 | 4.355 | 4.072 | 4.609 |

### 4.1.2 Estimation of $\eta$ as a function of the temperature via enthalpy evaluation

Let us consider the REDOX reaction (1). At equilibrium, the Gibbs free energy balance for the reaction as a function of temperature[33] reads as

$$G_{DEA*} - (G_{CO_2} + G_{DEA}) = 0, \tag{31}$$

where the molar free energies involved can be written as

$$G_{CO_2} = (G_{CO_2})_0 + RT \ln(p x_{CO_2}/p_0) \tag{32}$$

$$G_{DEA} = (G_{DEA})_0 + RT\ \ln(1-\theta) \tag{33}$$

$$G_{DEA^*} = (G_{DEA^*})_0 + RT \ln\theta. \tag{34}$$

Notice that in equations 33 and 34, we have introduced $\theta$ and $(1-\theta)$ as proportional to DEA* and DEA concentration respectively. Now, defining

$$(\Delta G_r)_0 := (G_{DEA^*})_0 - (G_{DEA})_0 - (G_{CO_2})_0 \tag{35}$$

and keeping (32)-(34) in mind, the equilibrium condition (31) gives

$$\ln\left(\frac{\theta}{1-\theta}\frac{p_0}{p x_{CO_2}}\right) = -\frac{(\Delta G_r)_0}{RT}. \tag{36}$$

Hence

$$\theta_{eq} = \theta_\infty = \frac{e^{-\frac{(\Delta G_r)_0}{RT}} p x_{CO_2}}{e^{-\frac{(\Delta G_r)_0}{RT}} p x_{CO_2} + p_0}. \tag{37}$$

Comparing (37) to (26) and assuming $p = p_0$ yields

$$K_{eq}(T) := e^{-\frac{(\Delta G_r)_0}{RT}} \ = \ \eta\, T_0/T. \tag{38}$$

Therefore, estimates of $K_{eq}(T)$ can be obtained from the estimates of the ratio $k_{abs}/k_{des}$ obtained in the previous section. For instance, the values of $\overline{\eta}(T)$ in Table 6 yield the values of $ln\left(K_{eq}(T)\right)$ given in Table 7. Since the temperature range is not wide, Van't Hoff's theory[34,35] holds: if $(\Delta H)_0$ is the standard enthalpy variation of reaction (1), then

$$\frac{(\Delta G_r)_0}{RT} = \frac{(\Delta H_r)_0}{RT}. \tag{39}$$

Therefore, the diagram of $ln(K_{eq}(T))$ against $T_0/T$ has to be a straight line, with slope $-\frac{(\Delta H)_0}{RT_0}$. Indeed, the points associated to the three temperatures $T_1 = 40$ °C, $T_2 = 60$ °C and $T_3 = 85$ °C in

Table 7: $ln\left(K_{eq}(T)\right)$ Versus the ratio $T_0/T$

| Temperature | $T_0/T$ (K/K) | $K_{eq}$ | $ln\left(K_{eq}\right)$ |
|---|---|---|---|
| $T_0 = 25\ ^\circ$C | 1 | 100.419 | 4.6094 |
| $T_1 = 40\ ^\circ$C | 0.95 | 55.4665 | 4.0158 |
| $T_2 = 60\ ^\circ$C | 0.89 | 16.3685 | 2.7954 |
| $T_3 = 85\ ^\circ$C | 0.83 | 3.8369 | 1.3447 |

Table 7 lie within a good approximation on the straight line

$$\ln\left(K_{eq}\right) = 22.335 T_0/T - 17.229, \tag{40}$$

with a correlation coefficient $R_{cor}$ = 0.9994; therefore,

$$|\Delta H_r|_0 = 22.335 \cdot T_0 R = 55.4 \cdot 10^3 \text{kJ/kmol}, \tag{41}$$

so, for 1 kg $CO_2$, $|\Delta H_r|_{mass} = |\Delta H_r|/44 = 1300$kJ/kg. Of course, one can add the point associated to temperature $T_0$ =25 $^\circ$C in such computation; the corresponding points are still aligned on a straight line, with a slightly lower correlation coefficient ($R_{cor}$ = 0.9862); this seems to be due to the fact that at about 27 $^\circ$C the DEA modifies its crystalline structure.

Finally, one can derive $\eta(T)$ as a function of the temperature, we recall[34] that, at constant pressure, the relation

$$T\left[\frac{\partial\left(\frac{\Delta G_r}{T}\right)}{\partial T}\right]_p = -\frac{\Delta H_r}{T} \tag{42}$$

holds. Integrating (36) and taking care of (39) and (42), the expression of $\eta(T)$ can be found:

$$\eta\left(T\right) = \left(T/T_1\right) \cdot \eta\left(T_1\right) e^{\frac{(\Delta H_r)_0}{RT_1}\left(1-\frac{T_1}{T}\right)}, \tag{43}$$

where $\eta(T_1) = 58.257$ and $(\Delta H_r)_0 = -55.4 \cdot 10^6$ J/kmol.

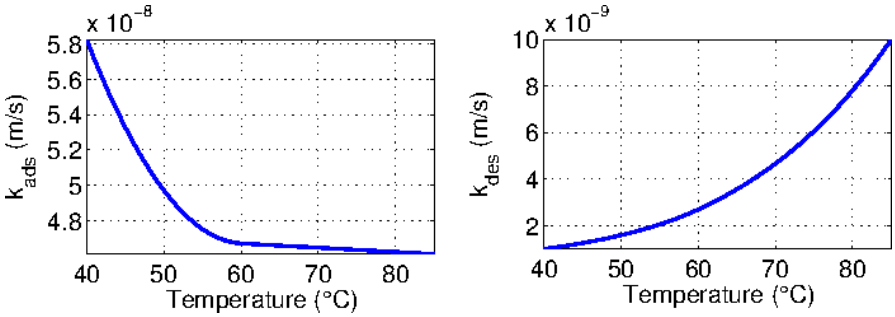


Figure 6: The identified $k_{abs}$ and $k_{des}$ as functions of temperature

## 4.2 Step 2: kinetic parameters evaluation from transient tests

In order to determine $k_{abs}(T)$ and $k_{des}(T)$ separately, three dynamic tests have been carried out, with inlet $CO_2$ molar fraction equal to 0.1 and at 40 °C, 60 °C and 85 °C temperature respectively. As in the steady-state tests, both the $CO_2$ molar fraction at the reactor outlet and the sorbent temperature at the reactor centre are the available measures.

An optimization procedure has been adopted, in order to find $k_{abs}$ (and therefore $k_{des}$ as $k_{abs}/\eta$) so as to minimize the error, in terms of $CO_2$ outlet molar fraction, between simulation results and process data in each of the three tests, while fulfilling the following monotonicity constraints on functions $k_{abs}(T)$ and $k_{des}(T)$: $k_{abs}(T)$ has to decrease with increasing temperature, while $k_{des}(T)$ has to increase with increasing temperature. Figure 6 reports the plots of the thus identified functions $k_{abs}(T)$ and $k_{des}(T)$.

## 4.3 Step 3: model validation

The identified model has been validated by comparing transient simulation results to experimental transient data; of course such comparison is performed by considering experiments different from those used in the identification procedure of Section 4.1.2. To be precise, we have performed the following tests associated to step responses against $CO_2$ inlet molar fraction variations:

- test 1: 5% inlet $CO_2$ molar fraction, 40 °C temperature in the absorption phase;
- test 2: 25% inlet $CO_2$ molar fraction, 60 °C temperature in the absorption phase;

- test 3: 25% inlet $CO_2$ molar fraction, 85 °C temperature in the absorption phase.

The experimental $CO_2$ outlet molar fraction transients are compared with the corresponding transients provided by our model in 7. As can be seen, the model is able to reproduce the real transients in all working conditions with satisfactory matching. Model adherence to the system behaviour could be increased by further improving parameter tuning. Several parameters in the model, in fact, such as the bulk and the pellet void fraction values, the active surface per sorbent unit volume and the heat exchange coefficients, have been taken from literature data so far, and thus they are subject to non-negligible uncertainty.

**Remark 1 (Model parameters updating)** *One of the main problems in the industrial use and control of the reactor for $CO_2$ absorption/desorption is the constant wear of the reactor during its life, which may cause the identified model parameters to become obsolete in the long run. In other words, the model returned by designers when the reactor is built may be no longer valid after the reactor has been used for a certain period of time. Hence, in principle, the procedure for parameter estimation should be repeated from time to time when the operating conditions have been subject to change. The procedure described in this Section, however, has the drawback that requires specific experiments on the plant and the intervention of qualified personnel to properly interpret the data. Thus, altogether, this makes the use of this procedure not feasible for the end user.*

*In recent years, a new parameter estimation technique, which is called the Two-Stage (TS) method, has been proposed in the specialized literature with the purpose of facing proper the issue of model parameters updating.[36] Specifically, the TS method is highly automated, so as to not require the intervention of qualified personnel, and can be easily reused by the end user whenever the model parameters need to be re-estimated. To be tuned for the specific problem at hand, the TS method requires a reliable physical model of the reactor along with a range of possible values for the uncertain parameters. Hence, tuning relies on the modeling and parameter identification previously discussed. Once tuned, from the end user perspective, the TS method accepts as input the data collected from a simple experiment on the plant in normal operating*

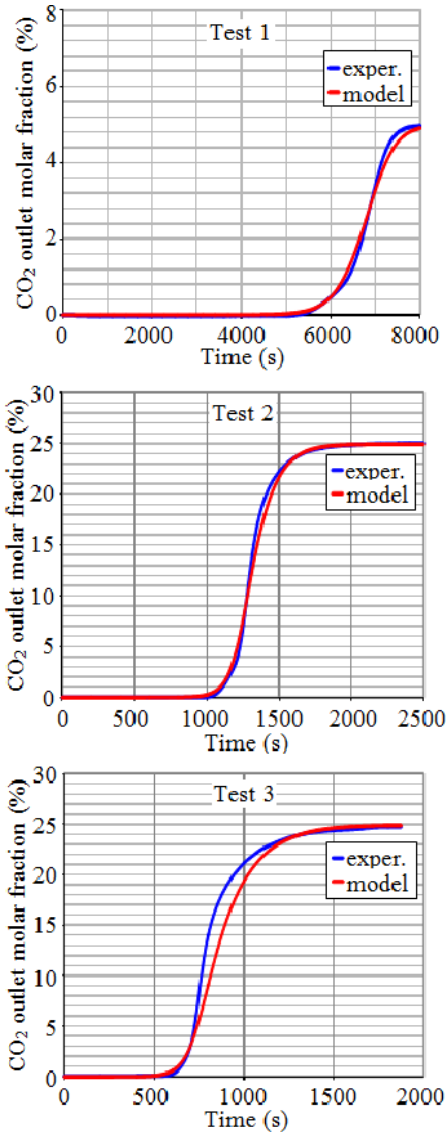


Figure 7: Experimental data (blue) Versus model output (red): $CO_2$ outlet molar fraction in the three validation tests

*conditions, and returns as output the new estimated values for the uncertain parameters, without any kind of human intervention. Moreover, the parameter estimates are obtained at very low computational cost, making the use of TS simple and effective.*

*The interested reader is referred to A, where more details on the TS method are given, along with an example of application to the reactor for $CO_2$ absorption/desorption.*

# 5 Conclusions

The dynamics of a $CO_2$ capture process based on amines supported on solid pellets have been studied, leading to a PDE and an ODE descriptions. The two main uncertain parameters in the model are the $CO_2$-amine reaction kinetic parameters. We have provided an identification method based on physical reasoning and a technique for the automatic update of their estimates, which have proven a good estimation capability with respect to lab-scale experimental data.

The model developed in this work will be employed to study the operating procedures and to design controllers of pilot-scale plants where the solid sorbent-anchored amine process is devoted to $CO_2$ capture not only from coal combustion flue gases, but also in biogas upgrading to biomethane.

# A The Two-Stage(TS) method for model parameters updating

In this Appendix we briefly describe the Two-Stage (TS) method,[36] a new parameter estimation technique which is specifically tailored to model parameters updating, as discussed in Remark 1. The method is based on an intensive offline simulation procedure, which analyzes the behaviour of the physical model we have developed in Section 2 while spanning across a range of parameters defined from the values estimated by the procedure described in Section 4. Hence, the TS method synergically builds up on the findings of this paper.

The method is outlined in A.1, while numerical results for the $CO_2$ absorption/desorption reactor are reported in A.2.

## A.1 Problem setting and description of the TS method

To introduce the TS method, we need rethinking to the model identification problem in a new perspective. We rely on the physical model introduced in the previous sections. The uncertainty can be restricted to the kinetic parameters. Since the ratio $k_{abs}/k_{des}$ can be considered as a reliable identified value, we can take the $k_{abs}(T)$ as the unique uncertain parameter. As seen in Section 4

(Figure 7), this parameter depends upon the temperature in a quadratic way. Therefore, we can set

$$k_{abs}(T) = aT^2 + bT + c \tag{44}$$

from the beginning. In conclusion, once the parameter vector $p = [a\ b\ c]'$ is determined, then the plant behaviour is completely described by the model introduced in Section 2. The parameter estimation problem, then, is that of retrieving the value of $p$ based on measurements of properly chosen input/output signals.

The solution of an estimation problem is an estimation algorithm, also called estimator, which is nothing but a suitable function $\widehat{f}:\ \mathbb{R}^{2N} \to \mathbb{R}^3$ which maps the measured observations

$$\bar{D}^N = \{\bar{y}(1), \bar{u}(1), \bar{y}(2), \bar{u}(2), \ldots, \bar{y}(N), \bar{u}(N)\}$$

into an estimate for the uncertain parameter:

$$\widehat{p} := \widehat{f}(\bar{y}(1), \bar{u}(1), \ldots, \bar{y}(N), \bar{u}(N)).$$

In standard approaches, like those based on Kalman filtering or Prediction Error Methods (PEM) in system identification,[37,38] the map $f$ is *implicitly* defined by means of some estimation criterion. This, however, poses some difficulties in using these approaches repeatedly (see Garatti and Bittanti[36] for the details).

The TS approach develops along completely different ideas: it resorts to off-line intensive simulation runs in order to explicitly reconstruct a function $\widehat{f}: \mathbb{R}^{2N} \to \mathbb{R}^3$ mapping measured input/output data into a parameter estimate $\widehat{p}$.

To be precise, we use the *simulator* of the reactor to generate input/output data for a number of different values of the unknown parameter $p$ chosen so as to densely cover a certain range of interest.

That is, we collect $N$ simulated measurements

$$D_1^N = \{y^1(1), u^1(1), \ldots, y^1(N), u^1(N)\}$$

for $p = p_1$; $N$ simulated measurements

$$D_2^N = \{y^2(1), u^2(1), \ldots, y^2(N), u^2(N)\}$$

for $p = p_2$; and so forth and so on, so as to work out a set of, say $m$, pairs $\{p_i, D_i^N\}$ as summarized

Table 8: The simulated data chart as the starting point of the two-stage method.

| | |
|---|---|
| $p_1$ | $D_1^N = \{y^1(1), u^1(1), \ldots, y^1(N), u^1(N)\}$ |
| $p_2$ | $D_2^N = \{y^2(1), u^2(1), \ldots, y^2(N), u^2(N)\}$ |
| $\vdots$ | $\vdots$ |
| $p_m$ | $D_m^N = \{y^m(1), u^m(1), \ldots, y^m(N), u^m(N)\}$ |

in Table 8. Such set of data is referred to as the *simulated data chart*.

From the simulated data chart, the function $\widehat{f}$ is reconstructed as that map minimizing the estimation error over simulated data, i.e.

$$\widehat{f} \leftarrow \min_{f \in \mathscr{F}} \frac{1}{m} \sum_{i=1}^{m} \left\| p_i - f(y^i(1), u^i(1), \ldots, y^i(N), u^i(N)) \right\|^2, \tag{45}$$

where $\mathscr{F}$ is a class of fitting functions. Should $\widehat{f}$ be found, then the true parameter vector corresponding to the actual measurements, say $\overline{D}^N = \{\overline{y}(1), \overline{u}(1), \ldots, \overline{y}(N), \overline{u}(N)\}$, can be estimated as

$$\widehat{p} = \widehat{f}(\overline{y}(1), \overline{u}(1), \ldots, \overline{y}(N), \overline{u}(N)).$$

Solving (45) is of course very critical, because of the high dimensionality of the problem: $f$ depends upon $2N$ variables, normally a very large number if compared to the number $m$ of experiments. In the TS approach, the resolution of (45) is split into two stages. This splitting is the key to obtain a good estimator $\widehat{f}$.

We now describe the two stages. The interested reader is referred to Garatti and Bittanti [36] for the full details.

**First stage.** The first step consists of a compression of the information conveyed by input/output sequences $D_i^N$, in order to obtain new data sequences $\widetilde{D}_i^n$ of reduced dimensionality. While in the data $D_i^N$ the information on the unknown parameter $p_i$ is scattered in a long sequence of $N$ samples, in the new compressed artificial data $\widetilde{D}_i^n$ such information is contained in a short sequence of $n$ samples ($n \ll N$). This leads to a new compressed artificial data chart composed of the pairs

Table 9: The compressed artificial data chart.

| | |
|---|---|
| $p_1$ | $\widetilde{D}_1^n = \{\alpha_1^1, \ldots, \alpha_n^1\}$ |
| $p_2$ | $\widetilde{D}_2^n = \{\alpha_1^2, \ldots, \alpha_n^2\}$ |
| $\vdots$ | $\vdots$ |
| $p_m$ | $\widetilde{D}_m^n = \{\alpha_1^m, \ldots, \alpha_n^m\}$ |

$\{p_i, \widetilde{D}_i^n\}$, $i = 1, \ldots, m$, see Table 9.

Each compressed artificial data sequence $\widetilde{D}_i^n$ is obtained by fitting a *simple black-box* model to each sequence $D_i^N = \{y^i(1), u^i(1), \ldots, y^i(N), u^i(N)\}$, and, then, by taking the parameters of this identified model, say $\alpha_1^i, \alpha_2^i, \ldots, \alpha_n^i$, as compressed artificial data, i.e. $\widetilde{D}_i^n = \{\alpha_1^i, \ldots, \alpha_n^i\}$.

It is worth noticing that the simple model used to fit the artificial data plays a purely instrumental and intermediary role. Hence, it is not required to have any physical meaning, nor it does matter if it does not tightly fit the data sequences $D_i^N$, as long as the $\alpha_1^i, \alpha_2^i, \ldots, \alpha_n^i$ reflect the variability of the $p_i$.

Summarizing, in the first stage a function $\widehat{g} : \mathbb{R}^{2N} \to \mathbb{R}^n$ is found, transforming each simulated data sequence $D_i^N$ into a new sequence of compressed artificial data $\widetilde{D}_i^n$ still conveying the information on $p_i$. The function $\widehat{g}$ is defined by the chosen class of simple models used to fit simulated data along with the corresponding identification algorithm.

**Second stage.** Once the compressed artificial data chart in Table 9 has been worked out, prob-

lem (45) becomes that of finding a map $\widehat{h}:\mathbb{R}^n \to \mathbb{R}^q$ which fits the $m$ compressed artificial observations into the corresponding parameter vectors, i.e.

$$\widehat{h} \leftarrow \min_{h\in\mathscr{H}} \frac{1}{m}\sum_{i=1}^{m} \left\| p_i - h(\alpha_1^i,\ldots,\alpha_n^i)\right\|^2, \tag{46}$$

where $\mathscr{H}$ is a suitable function class.

Problem (46) is reminiscent of the original minimization problem in (45). However, being $n$ small thanks to the compression of the information in the first stage, the resolution of (46) is not problematic anymore. One can e.g. resort to Neural Networks and solve (46) by means of the standard algorithms developed for fitting this class of nonlinear functions to the data.

**Use of the two-stage method.** After $\widehat{h}$ has been computed, the final estimator $\widehat{f}$ mapping input/output data into the parameter estimate $\widehat{p}$ is obtained as

$$\widehat{f} = \widehat{h}\circ\widehat{g} = \widehat{h}(\widehat{g}(\cdot)),$$

i.e. as the composition of $\widehat{g}$ and $\widehat{h}$.

Note that $\widehat{f}$ is constructed off-line, by means of simulation experiments only. However, when a real input/output sequence $\bar{D}^N = \{\bar{y}(1),\bar{u}(1),\ldots,\bar{y}(N),\bar{u}(N)\}$ is collected, the unknown parameter vector can be estimated as $\widehat{p} = \widehat{h}(\widehat{g}(\bar{D}^N))$, that is, by evaluating $\widehat{f}$ in correspondence of the actually seen data sequence. This evaluation can be easily performed by an automatic device, which can be used to generate estimates $\widehat{p}$ whenever it is needed, at very low computational cost and without any intervention of specialized personnel.

## A.2 Application to the reactor model: results

As we have seen, the TS method is based on the execution of intensive simulation trials of the physical model. This simulation phase is performed offline and need not to be repeated along the plant life. When data from a new experiments are available, the algorithms builds the new

parameter estimates very fast.

We now describe the offline procedure for the tuning of the TS algorithm to the $CO_2$ absorption/desorption reactor. We also give some simulation results demonstrating the effectiveness of the approach.

In 4 we estimated the kinetic absorption parameter for the temperatures $T_1 = 40^\circ$C, $T_2 = 60^\circ$C, $T_3 = 85^\circ$C:

$$\bar{k}_{abs}(T_1) = 5.8257 \times 10^{-8} m/s,$$

$$\bar{k}_{abs}(T_2) = 4.6707 \times 10^{-8} m/s,$$

$$\bar{k}_{abs}(T_3) = 4.6105 \times 10^{-8} m/s.$$

Starting from values $\bar{k}_{abs}(T_i)$, $i = 1,2,3$, we construct a range of possible values around them as follows:

$$0.5\bar{k}_{abs}(T_i) \leq k_{abs}(T_i) \leq 2\bar{k}_{abs}(T_i), \quad i = 1,2,3,$$

In view of expression (44), these bounds on $k_{abs}$ define feasible regions for the triple of parameters $p = [a\ b\ c]'$.

At this point we are in a position to define the simulation experiments we have performed. To be precise, we have extracted $m = 2500$ random values for $p = [a\ b\ c]'$, ensuring that the corresponding $k_{abs}$ meet the above bounds.

Correspondingly, we ran 2500 simulations of the reactor, each time injecting a $CO_2$ molar fraction step of 10% as the input, starting from steady-state conditions at an initial temperature $T = 60$ °C. As the output signal we have considered temperature at the beginning of the reactor (point A in 3). Typical temperature outputs for three values of the parameter vector $p$ are depicted in Figure 8. By sampling at $0.025Hz$ the input and output signals, we obtained 2500 input/output sequences each $N = 150$ samples long:

$$u^i(1), y^i(1), u^i(2), y^i(2), \ldots, u^i(150), y^i(150),$$

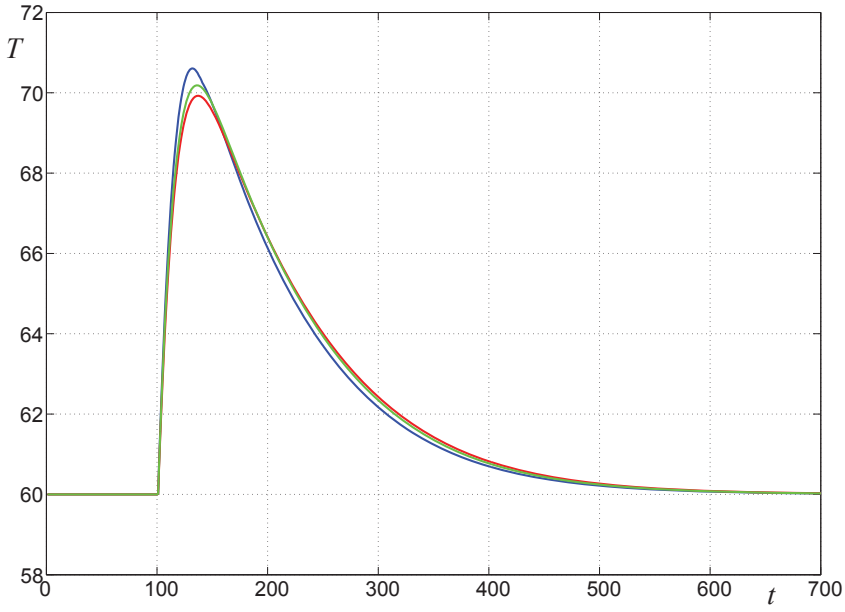


Figure 8: Typical temperature diagrams at point A (reactor inlet) while injecting an inlet $CO_2$ molar fraction step.

$i = 1,2,\ldots,2500$. These sequences together with the 2500 extracted values for $p$ formed the simulated data chart.

As for the generation of the compressed artificial data chart, we noticed that, in our experiments, the output looks like an impulse response, because of the zero in the origin introduced by the external refrigerator, which forces the temperature to return to the initial value. Hence, by letting $\Delta u^i(t) = u^i(t) - u^i(t-1)$ be the impulse corresponding to the given step, we fitted to each generated data sequence a low-order state-space model

$$\begin{aligned} x(t+1) &= Fx(t) + G\Delta u^i(t) \\ y^i(t) &= Hx(t), \end{aligned}$$

by using the Ho-Kalman algorithm.[39] To be precise we have considered a third order system, so that the total number of entries in the triple $(F,G,H)$ is 15. These entries are the parameters we have used as compressed artificial data $\alpha_1^i, \alpha_2^i, \ldots, \alpha_{15}^i$, $i = 1,2,\ldots,2500$.

The final estimator $\widehat{h}(\alpha_1^i, \alpha_2^i, \ldots, \alpha_{15}^i)$ was instead derived by resorting to a feed-forward 3-layers

neural network, with 20 neurons in each hidden layer.[40] The network weights were trained by the usual back-propagation algorithm. The order of the state-space model as well as that of the neural network were eventually chosen by means of cross-validation.

In order to test the TS estimator, we picked 500 new random values for the uncertain vector parameter $p$, and correspondingly we ran new 500 simulations of the reactor model in the same experimental conditions as in the training phase. The 500 data sequences obtained by sampling input and output signals at $0.025Hz$ were made available to the TS estimator so as to generate 500 estimates of the parameter vector $p$. These estimates were eventually compared to the true values of the parameter vector so as to evaluate the performance of the obtained estimator (cross-validation).

In Figure 9, the estimates $\hat{a}$, $\hat{b}$, and $\hat{c}$, respectively, as returned by the TS estimator, are plotted against the true parameter values $a$, $b$, and $c$. That is, with reference, e.g., to the first box at the top, the $x$-axis of each plotted point is the extracted value for the parameter $a$, while the $y$-axis is the corresponding estimate supplied by the TS estimator. The same interpretation holds for the other figures. Clearly, the closer the points to the graph bisector, the better the estimator.

As it appears, the figures reveal a great estimation capability of the TS estimator, especially as for parameters $b$ and $c$, while parameter $a$ is less identifiable. Overall, the estimation results are quite good, and the TS approach was able to produce an explicit estimator map $\widehat{f}(\cdot) = \widehat{h}(\widehat{g}(\cdot))$, defined as the composition of the Ho-Kalman algorithm and the trained neural network, which can be used over and over to generate suitable estimates of $p$ whenever a tuning of the reactor model is needed.

## Acknowledgement

This work has been financed by the Research Fund for the Italian Electrical System under the Contract Agreement between RSE S.p.A. and the Ministry of Economic Development - General Directorate for Nuclear Energy, Renewable Energy and Energy Efficiency in compliance with the Decree of March 8, 2006. The support by the MIUR national project “Identification and adaptive

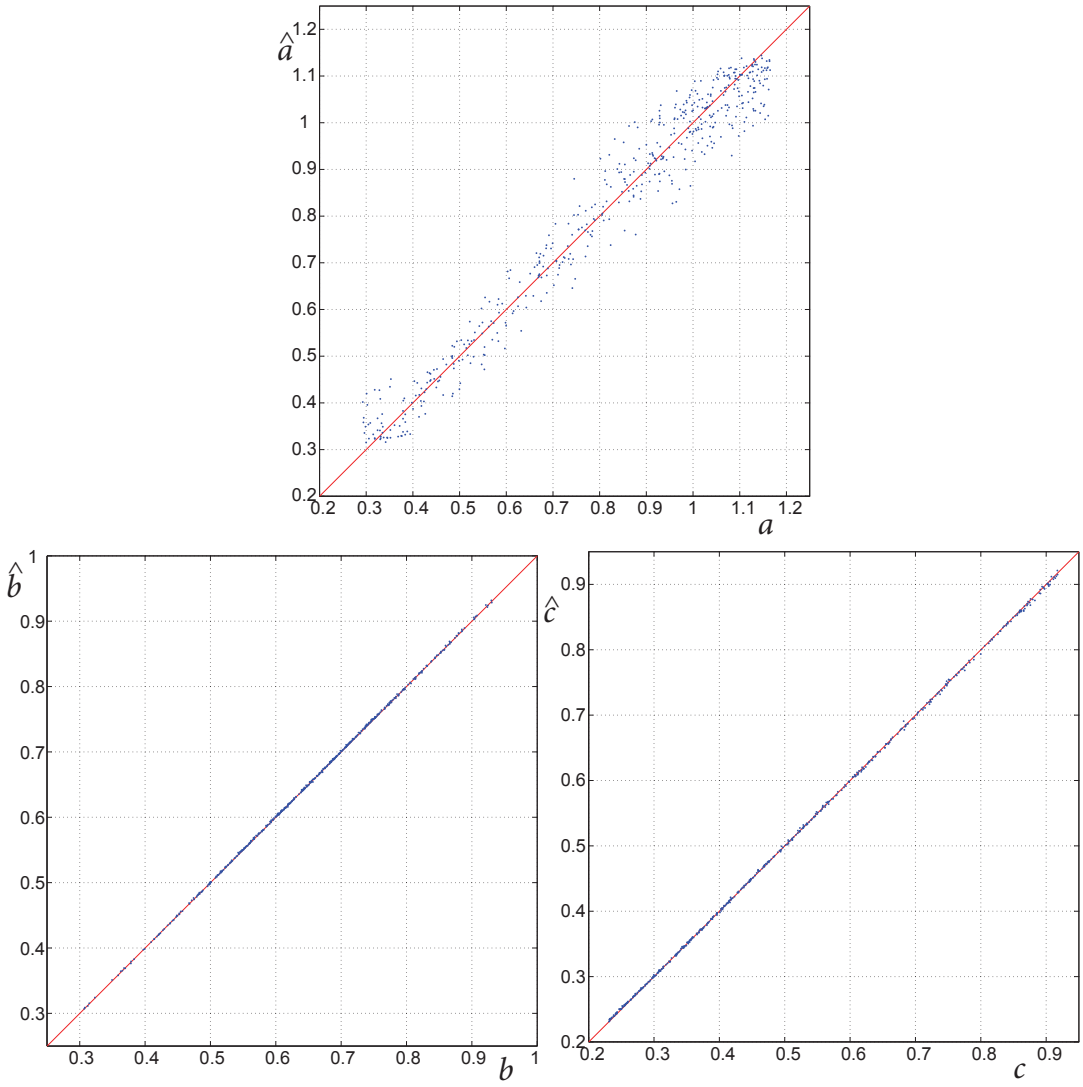


Figure 9: Estimation results for parameters *a*, *b*, and *c*.

control of industrial systems" and by CNR - IEIIT is also gratefully acknowledged.

## References

1. Ciferno, J. P.; Ramezan, M.; Skone, J.; ya Nsakala, N.; Liljedahl, G. N.; Gearhart, L. E.; Hestermann, R.; Rederstorff, B. *Carbon Dioxide Capture from Existing Coal-Fired Power Plants* [Online]; DOE/NETL-401/110907; DOE/NETL Report, 2007. http://www.netl.doe.gov/File Library/Research/Energy Analysis/Publications/CO2-Retrofit-From-Existing-Plants-Revised-November-2007.pdf (accessed September 4, 2014).

2. Herzog, H. *An Introduction to $CO_2$ Separation and Capture Technologies*; MIT Energy Laboratory, 1999.

3. Spigarelli, B. P.; Kawatra, S. K. Opportunities and challenges in carbon dioxide capture. *J. $CO_2$ Util.* **2013**, *1*, 69–87.

4. Veawab, A.; Tontiwachwuthikul, P.; Chakma, A. Corrosion behaviour of carbon steel in the $CO_2$ absorption process using acqueous amine solutions. *Ind. Eng. Chem. Res.* **1999**, *38*, 3917–3924.

5. Serna-Guerrero, R.; Da'na, E.; Sayari, A. New insights into the interactions of $CO_2$ with amine-functionalized silica. *Ind. Eng. Chem. Res.* **2008**, *47*, 9406–9412.

6. Knudsen, J. N.; Jensen, J. N.; Vilhelmsen, P. J.; Biede, O. Experience with $CO_2$ capture from coal flue gas in pilot-scale: Testing of different amine solvents. *Energy Procedia* **2009**, *1*, 783–790.

7. Goff, G. S.; Rochelle, G. T. Monoethanolamine degradation: $O_2$ mass transfer effects under $CO_2$ capture conditions. *Ind. Eng. Chem. Res.* **2004**, *43*, 6400–6408.

8. Herzog, H.J.; Drake, E. M. *Long-Term Advanced $CO_2$ Capture Options*; IEA/93/OE6; IEA Greenhouse Gas R&D Programme: Cheltenham, UK, 1993.

9. Zhao, L.; Riensche, E.; Blum, L.; Stolten, D. How gas separation membrane competes with chemical absorption in postcombustion capture. *Energy Procedia* **2011**, *4*, 629–636.

10. Favre, E.; Bounaceur, R.; Roizard, D. A hybrid process combining oxygen enriched air combustion and membrane separation for post-combustion carbon dioxide capture. *Sep. Purif. Technol.* **2009**, *68*, 30–36.

11. Sjostrom, S.; Krutka, H. Evaluation of solid sorbents as a retrofit technology for $CO_2$ capture. *Fuel* **2010**, *89*, 1298–1306.

12. Krutka, H.; Sjostrom, S. *Evaluation of Solid sorbents as a Retrofit Technology for $CO_2$ Capture from Coal-Fired Power Plants* [Online]; Final technical report; DOE Award Number DE-NT0005649; Report Number 05649FR01; 2011. http://www.netl.doe.gov/File Library/Research/Coal/ewr/co2/evaluation-of-solid-sorbents-nov2011.pdf (accessed September 4, 2014).

13. Zhao, W.; Zhang, Z.; Li, Z.; Cai, N. Investigation of thermal stability and continuous $CO_2$ capture from flue gases with supported amine sorbent. *Ind. Eng. Chem. Res.* **2013**, *52*, 2084–2093.

14. Samanta, A.; Zhao, A.; Shimizu, G. K. H.; Sakar, P.; Gupta, R. Post-Combustion $CO_2$ Capture Using Solid Sorbents: a Review. *Ind. Eng. Chem. Res.* **2012**, *51*, 1438–1463.

15. Gray, M. L.; Hoffman, J. S.; Hreha, D. C.; Fauth, D. J.; Hedges, S. W.; Champagne, K. J.; Pennline, H. W. Parametric Study of Solid Amine Sorbents for the Capture of Carbon Dioxide. *Energy Fuels* **2009**, *23*, 4840–4844.

16. Mazzocchi, L.; Notaro, M.; Alvarez, M.; Ballesteros, J. C.; Burgos, S.; Pardos-Gotor, J. M. *Preparation and laboratory tests of low cost solid sorbents for post-combustion $CO_2$ capture.* Proceedings of the International conference on Sustainable Fossil Fuels for Future Energy - S4FE2009, Rome, Italy, Jul 6-10, 2009.

17. Notaro, M.; Savoldelli, P.; Valli, C. *Tests on Solid Sorbents for Post-Combustion $CO_2$ Capture and Feasability of a Pilot Application* [Online]; Technical report; 2008; in Italian. http://www.ricercadisistema.it (accessed September 4, 2014).

18. Notaro, M.; Pinacci, P. *Carbon dioxide capture from flue gas by solid regenerable sorbents.* Proceedings of the 3rd International Conference on Clean Coal Technologies for our Future, Cagliari, Italy, May 15-17, 2007.

19. Notaro, M.; Pardos Gotor, J. M.; Savoldelli, P. Method for capturing $CO_2$. 2012; WO Patent

App. PCT/ES2012/070,137. http://www.google.com/ patents/WO2012120173A1?cl=en (accessed September 4, 2014).

20. Notaro, M. *Post-combustion $CO_2$ capture by solid sorbents.* In Convegno nazionale AEIT 2011, Milan, Italy, Jun 27-29, 2011; in Italian.

21. Bittanti, S.; Calloni, L.; De Marco, A.; Notaro, M.; Prandoni, V.; Valsecchi, A. *A process for $CO_2$ post combustion capture based on amine supported on solid pellets.* Proceedings of the 8th IFAC International Symposium on Advanced Control of Chemical Processes, Furama Riverfront, Singapore, Jul 10-13, 2012.

22. Finlayson, B. A. Packed bed reactor analysis by orthogonal collocation. *Chem. Eng. Sci.* **1971**, *26*, 1081–1091.

23. Santacesaria, E.; Morbidelli, M.; Servida, A.; Storti, G.; Carrà, S. Separation of Xylenes on Y Zeolites. Note II: Breakthrough Curves and Their Interpretation. *Ind. Eng. Chem., Process Des. Develop.* **1982**, *21*, 446–451.

24. Bisone, L.; Bittanti, S.; Canevese, S.; De Marco, A.; Garatti, S.; Notaro, M.; Prandoni, V. *Modeling and parameter identification for $CO_2$ post-combustion capture by amines supported on solid sorbents.* Proceedings of the 19th IFAC World Congress, Cape Town, South Africa, Aug 24-29, 2014.

25. Foo, K. Y.; Hameed, B. H. Insights into the modeling of adsorption isotherm systems. *Chem. Eng. J.* **2010**, *156*, 2–10.

26. Ruthven, D. M. *Principles of Adsorption and Adsorption Processes*; John Wiley & Sons: New York, 1984.

27. Ruthven, D. M.; Farooq, S.; Knaebel, K. S. *Pressure Swing Adsorption*; VCH: New York, 1994.

28. Bird, R. B.; Stewart, W. E.; Lightfoot, E. N. *Transport phenomena*; Wiley: New York, 1960.

29. Froment, G. F.; Bischoff, K. B. *Chemical Reactor Analysis and Design*, 2nd ed.; John Wiley & Sons: New York, 1990.

30. Balakrishnan, A. R.; Pei, D. C. T. Heat Transfer in Gas-Solid Packed Bed Systems. 1. A Critical Review. *Ind. Eng. Chem., Process Des. Develop.* **1979**, *18*, 30–40.

31. Mason, E. A.; Malinauskas, A. P.; Evans III, R. B. Flow and Diffusion of Gases in Porous Media. *J. Chem. Phys.* **1967**, *46*, 3199–3216.

32. Serna-Guerrero, R.; Sayari, A. Modeling adsorption of $CO_2$ on amine-functionalized mesoporous silica. 2: Kinetics and breakthrough curves. *Chem. Eng. J.* **2010**, *161*, 182–190.

33. Mahan, B. H. *University Chemistry*, 3rd ed.; Addison-Wesley Publishing Co.: Reading, 1975.

34. Barrow, G. M. *Physical Chemistry*, 5th ed.; McGraw-Hill: New York, 1988.

35. Atkins, P. W. *Physical Chemistry*, 5th ed.; Oxford University Press: Oxford, 1994.

36. Garatti, S.; Bittanti, S. A new paradigm for parameter estimation in system modeling. *Int. J. Adapt. Contr. Signal Process.* **2013**, *27*, 667–687.

37. Ljung, L. *System Identification: Theory for the User*, 2nd ed.; Prentice-Hall: Upper Saddle River, 1999.

38. Söderström, T.; Stoica, P. *System Identification*; Prentice-Hall: Englewood Cliffs, 1989.

39. Ho, B. L.; Kalman, R. E. Effective construction of linear state-variable models from input/output functions. *Regelungstechnik* **1966**, *14*, 545–592.

40. Haykin, S. *Neural Networks: A Comprehensive Foundation*, 2nd ed.; Prentice Hall: Upper Saddle River, 1998.